Modulation of a Photoswitchable Dual-Color Quantum Dot containing a Photochromic FRET Acceptor and an Internal Standard

ARTICLE *in* NANO LETTERS · JUNE 2012

Impact Factor: 13.59 · DOI: 10.1021/nl301093s · Source: PubMed

4 AUTHORS, INCLUDING:

Sebastian Diaz
United States Naval Research Laboratory
10 PUBLICATIONS **117** CITATIONS
SEE PROFILE

Luciana Giordano
National Scientific and Technical Research C…
18 PUBLICATIONS **501** CITATIONS
SEE PROFILE

NANO LETTERS

Letter

pubs.acs.org/NanoLett

Modulation of a Photoswitchable Dual-Color Quantum Dot containing a Photochromic FRET Acceptor and an Internal Standard

Sebastián A. Díaz,[†,‡] Luciana Giordano,[‡] Thomas M. Jovin,*[,‡] and Elizabeth A. Jares-Erijman[†]

[†]Departamento de Química Orgánica, Facultad de Ciencias Exactas y Naturales, Universidad de Buenos Aires, CIHIDECAR, CONICET, 1428 Buenos Aires, Argentina

[‡]Laboratory of Cellular Dynamics, Max Planck Institute for Biophysical Chemistry, Am Fassberg 11, 37077 Göttingen, Germany

Supporting Information

ABSTRACT: Photoswitchable semiconductor nanoparticles, quantum dots (QDs), couple the advantages of conventional QDs with the ability to reversibly modulate the QD emission, thereby improving signal detection by rejection of background signals. Using a simple coating methodology with polymers incorporating a diheteroarylethene photochromic FRET acceptor as well as a spectrally distinct organic fluorophore, photoswitchable QDs were prepared that are small, biocompatible, and feature ratiometric dual emission. With programmed irradiation, the fluorescence intensity ratio can be modified by up to ∼100%.

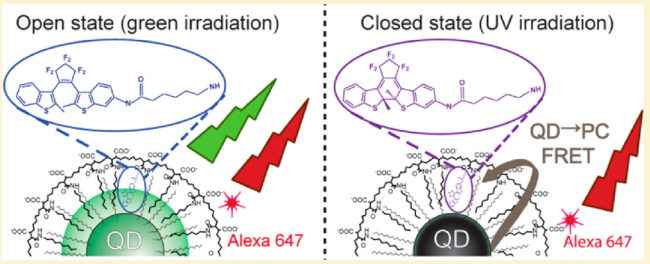

KEYWORDS: *Quantum dots, FRET, photochromism, internal standard, ratiometric imaging*

Since their inception semiconductor nanocrystals, or quantum dots (QDs), have been applied widely in biological imaging,[1] most recently for multiplexed analysis,[2] single particle imaging,[3] prolonged real-time visualization,[4] and super resolution microscopy.[5] QDs are particularly well suited to these tasks due to their broad excitation, narrow emission, photostability, and brightness. Despite their many virtues, colloidal QDs are generally synthesized in organic solvents and require surface modification in order to achieve solubility in aqueous media and biocompatibility. These aims are met either by replacing or by capping the original hydrophobic surface ligands,[6] techniques that also provide the main route to further functionalization of the QDs for targeting and multiparametric biosensing.[7,8]

Förster resonance energy transfer (FRET) is an efficient technique for the modulation of QD fluorescence.[9−12] Photochromic compounds (PCs) with two states differing in absorption properties have been introduced as FRET acceptors in a configuration we have previously termed pcFRET.[13−15] The system constitutes a reversible switch based on FRET under control by light. A very suitable family of photochromic compounds for pcFRET comprises the thiophene-based diheteroarylethenes,[16] introduced by Irie,[17,18] which have two thermally stable states (open form, oPC, and photocyclized closed form, cPC) that can undergo numerous photocycles without fatigue. The open form can assume antiparallel and parallel conformations of which only the former can undergo photocyclization. Several water-soluble diheteroarylethene PCs have been designed,[19,20] but they still require a hydrophobic microenvironment for optimum photoconversion.[21]

We have previously reported[22] the design of photoswitchable QDs (psQDs) based on the strategy introduced by the Parak laboratory[23] for solubilizing organic nanoparticles with coats of amphiphilic comb-polymers. [In referring to the previously reported psQD construct we will use the term Gen-1]. Such polymer-capped QDs have been targeted to biological applications in aqueous media.[24,25] The amphiphilic polymer can be functionalized both prior to or after nanoparticle coating[7] with various groups located either in the hydrophobic interior or hydrophilic exterior of the coating polymer. In our application, the wrapped QDs architecture permits placement of the PC molecules in the hydrophobic compartment demarcated by the outer surface of the semiconductor QD and the polymer cap.[22]

We report here a new structural design that creates a biocompatible photoswitchable QD with a secondary dye (Alexa Fluor647 cadaverine) acting as an internal standard and thus allowing dual-color, ratiometric sensing and imaging (Scheme 1). The psQD is smaller than other related constructs[26−30] (∼5 nm diameter by EM, a ∼14 nm hydrodynamic diameter; see Supporting Information), does not exhibit fatigue, and is readily photomodulatable, such that the emission can be externally controlled. The ratiometric signal changes by ∼100% and allows sensitive, selective detection by suppression of background and photobleaching contributions using phase-sensitive techniques. These can be applied in the steady-state[31] as well as in the nanoseconds

Received: March 21, 2012
Revised: May 15, 2012

dx.doi.org/10.1021/nl301093s | *Nano Lett.* XXXX, XXX, XXX−XXX

Scheme 1. Dual-Color psQD Schematic[a]

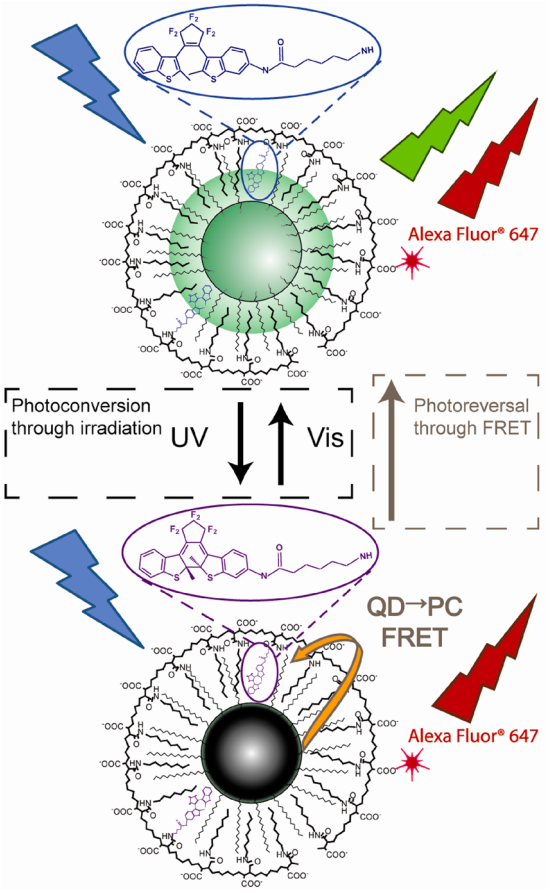

[a]The fluorescence of the QD is modulated by the photoconversion of the PC while the Alexa647 fluorescence is constant. The PC in the open form (oPC) is photoconverted with UV irradiation to the closed form (cPC), which can then be photoreversed by direct excitation with visible light, or via FRET from the QD acting as a donor.

Scheme 2. Spectral Signature of Dual-Color psQD Components and Chemical Architecture of Conjugated Polymer[a]

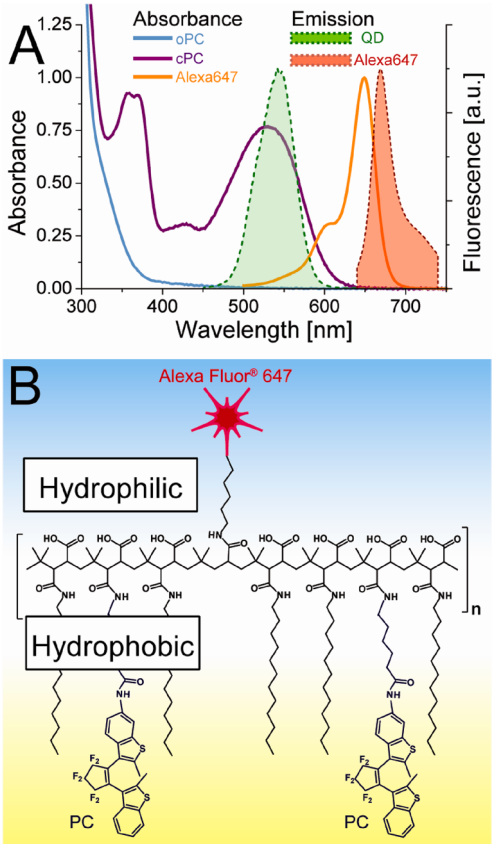

[a](A) Superposition of absorbance (solid lines) and emission (filled areas) spectra of PC, QD, and Alexa647, demonstrating the PC spectral overlap with the QD but not with the Alexa647. The spectra are normalized by their peak values. (B) Schematic of photochromic amphiphilic comb polymer doped with Alexa647.

regime,[32] in the latter case exploiting the different QD and Alexa647 fluorescence decay kinetics.

The preparation of the dual-color psQDs begins with the synthesis of the Alexa doped photochromic amphiphilic polymer (Scheme 2). Certain modifications of the methodology previously reported for dye-doped poly(maleic anhydride) based polymers[22,33,34] were required for introducing the double functionalization.

For the polymer synthesis 6 mg (1 μmole polymer, 40 μmoles monomer) of PMA (Sigma-531278, MW ~6000) was introduced into a dry 10 mL flask. Two milliliters of a DMF:DMSO solution of Alexa647 cadaverine (Invitrogen, A-30679; 0.16 μmoles, or 4 molecules per 1000 maleic anhydride monomers) were added. The solution was stirred at 60 °C for 90 min and then 7.7 mg (14 μmoles) of PCahx [6-amino-*N*-(3-(3,3,4,4,5,5-hexafluoro-2-(2-methylbenzo[b]thiophen-3-yl)-cyclopent-1-enyl)-2-methylbenzo[b]thiophen-6-yl)hexanamide; for synthetic details of PCahx see Supporting Information] was added in the minimal possible volume of tetrahydrofuran. The PCahx is a diheteroarylethene PC with a 6 carbon linker terminating in a primary amine. This linker positions the PC closer to the QD than in the Gen-1 psQD as well as increasing the yield of conjugation to the polymer. From prior experience with PCahx, we anticipated a conjugation yield of ~20%, corresponding to ~3 PC groups/polymer. We simplify the terminology by henceforth referring to PCahx as PC. Dodecylamine (1.85 mg, 10 μmoles) was added to the flask and the reaction was left overnight at 60 °C. An additional 3.7 mg (20 μmoles) of dodecylamine was added and allowed to react for 4 h. The product was purified and characterized as previously described.[22] The nomenclature adopted for the polymer product represents modifications to the polyisobutylene-alt-maleic anhydride backbone as percentages of anhydride rings coupled to the added molecules. Thus, the final polymer is denoted PMA 7PC 75C12 0.3Al; for every 1000 original maleic anhydride monomers there are 750 dodecylamine chains, ~70 PC molecules, and 3 Alexa647.

We utilized Series A CSS 540 nm QDs CdSe/CdS/ZnS core−shell−shell nanoparticles[35] (CAN GmbH, Hamburg) emitting at 540 nm and rendered soluble in organic solvents by lipophilic surface ligands (TOPO/TOP/HDA). The coated QDs were transferred to an aqueous medium and purified following a simple, previously reported methodology.[22] The polymer self-assembly is directed by interdigitations of the aliphatic chains with the lipophilic ligands on the QD surface. The PC is preferentially localized to the hydrophobic microenvironment established by the QD surface ligands and the dodecylamine chains of the polymer. The hydrophilic Alexa647 and pendant carboxylic groups are presumed to

dx.doi.org/10.1021/nl301093s | *Nano Lett.* XXXX, XXX, XXX−XXX

extend into the aqueous medium, conferring a negative surface charge and solubility to the nanoparticle. The final construct is denoted a dual-color psQD (dual-color photoswitchable quantum dot). The properties and data presented below were determined in 50 mM Na-borate buffer, pH 9.0, under aerobic conditions. Stability was maintained in the pH range 7−12 and no adverse effects were perceived upon lowering the salt concentration to 0.5 mM. The properties of the dual-color psQDs were unaltered after storage for 6 months.

The absorption and fluorescence spectra at 20 °C of dual-color psQDs were acquired on a Cary 100 UV−vis Spectrophotometer and a Cary Eclipse Fluorimeter (Varian), respectively. The concentrations of the nanoparticle solutions were in the range of 0.1−0.5 μM. For fluorescence measurements, the maximum absorbance of the solution was maintained at <0.1 to avoid internal filter effects and trivial reabsorption, and low levels of excitation light were utilized for monitoring the system so as to avoid photoconversion of the PCs. The phase transfer shifted the peak of the QD emission to 550 nm and led to a reduction of the quantum yield to 0.26, a value similar to that reported for other polymer-coated QDs.[36]

The photochrome composition of the dual-color psQD was determined by resolving the absorbance spectrum into its constituent contributions. The A_{525} of the dual-color psQDs with all the PC in the open form was assumed to originate exclusively from the semiconductor, thus permitting an estimation of the nanoparticle concentration. The increment in A_{540} upon UV irradiation was assigned to changes in the relative concentrations of oPC and cPC. The concentrations of cPC, and thus of total PC and number of PCs per QD, were obtained from the known differences in extinction coefficients and the cPC fraction in the photostationary state (α_{PS}, see below). The A_{650} originated solely from the Alexa647 and thus an Alexa647/QD ratio could also be computed. In interpreting the data, we assumed random distributions of the PC and reference probes on the polymer and of the polymer on the QD. The calculations yielded mean values of 1.2 ± 0.1 Alexa647 and 35 ± 1 PC per QD, corresponding to ∼400−500 monomers of polymer (or ∼10−13 polymers) per QD. The polymer content was one-half that of the Gen-1 psQD. The more efficient packing was reflected in the ease of QD coating and phase transfer. From the low value for Alexa647, the fractional distributions for QDs with 0, 1, 2 and >2 probes would be 0.30, 0.36, 0.22, and 0.12, respectively.

Scheme 2A shows the most pertinent spectral properties of the individual components of the dual-color psQD. The latter exhibited two emission wavelengths, 550 and 666 nm, corresponding to the QD and Alexa647, respectively. Both emissions could be elicited over a broad excitation band corresponding to the QD. As indicated above, QDs can act as FRET donors,[10,37−39] in this case not only to the PC groups but also to the Alexa647, which will thus exhibit emission upon excitation throughout the QD excitation band. The computed Förster transfer parameter[13] (R_o), the donor−acceptor distance for which the energy transfer efficiency is 0.5, are the following: QD-oPC, 1.3 nm; QD-cPC, 4.1 nm; QD-Alexa647: 4.1 nm, assuming two-thirds for the value of orientation factor κ^2. The similar values for QD-cPC and the QD-Alexa647 result from compensation of the lesser spectral overlap in the latter case by the much larger extinction coefficient of Alexa647, resulting in a similar overlap integral (J).[13]

We define an emission ratio (ER) as the Alexa647 emission at 666 nm divided by the QD emission at 550 nm. Alexa647 can be excited selectively from 580 to 660 nm. Thus, the ER is adjustable by selection of one or more excitation band(s). In the experiments described below, the selected excitation wavelengths of 400 and 600 nm were optimal in that they correspond to minima in the PC absorbance.

Reversible photoswitching of the PC probe in the dual-color psQD was achieved by alternating irradiation with UV light (340 ± 10 nm, 1.1 mW cm^{-2}) and visible/green light (545 ± 10 nm, 6.2 mW cm^{-2}). Sequential pulses (∼10 s) of either UV or visible light were utilized to achieve the two photostationary states,[14,22] the first consisting exclusively of oPC, and the second of a distribution between oPC and cPC established by UV irradiation. Further references to the photostationary state assume the latter condition. The changes in the absorbance and fluorescence spectra of the dual-color psQD upon passing from the open to the closed states are shown in Figure 1. The

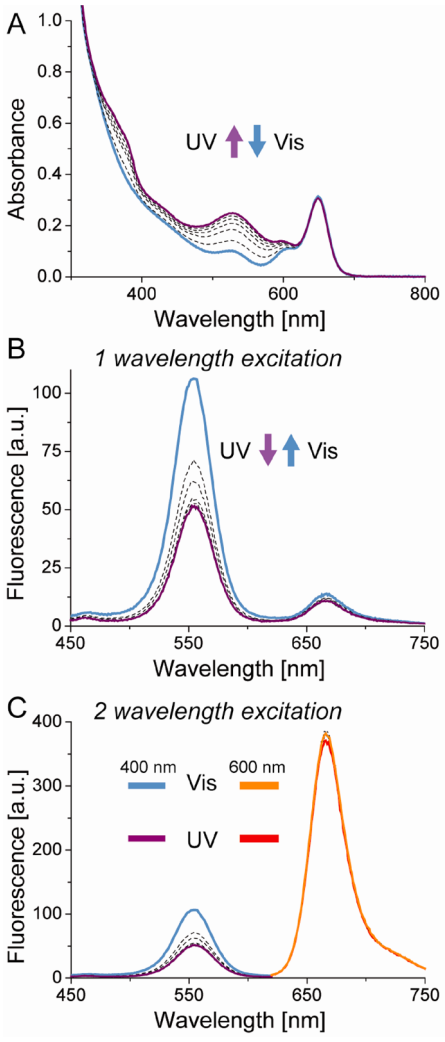

Figure 1. Spectroscopic monitoring of dual-color psQD. Irradiation consisted of consecutive 10 s pulses of either UV or visible light until no further change was observed; UV, 340 ± 10 nm (irradiance 1.1 mW cm^{-2}) and vis, 545 ± 10 nm (irradiance 6.2 mW cm^{-2}). Temperature, 20 °C. (A) Absorbance spectra (B) Fluorescence spectra of dual-color psQD with excitation at 400 nm. (C) Fluorescence spectra of dual-color psQD with excitation wavelength at 400 nm for QD detection and 600 nm for Alexa647 detection. The 600 nm excitations are represented by two colors (orange, red); the signals differed very slightly.

dx.doi.org/10.1021/nl301093s | Nano Lett. XXXX, XXX, XXX−XXX

photostationary state of PC conjugated to the polymer corresponds to a 22% conversion (α_{PS} = 0.22) of the open to the closed states (for calculations and details see Supporting Information 1B). The photoconversion process of the dual-color psQD is more complex due to the photoreversion caused by FRET from the QD to the cPC and the existence of two subpopulations differing in FRET efficiency (see below). Thus, the photostationary state corresponds to a lower α_{PS} than in the case of the free or polymer-conjugated PC (see calculations and discussion below).

The maximum observed quenching of fluorescence at the 550 nm peak upon exposure to UV light was 52% (mean 48 ± 2%). Irradiation with visible light restored the fluorescence to the initial state. Using a single excitation wavelength (400 nm), the ER changed from 0.13 to 0.22 (66% increase). By exciting both probes individually (QD at 400 nm, Alexa647 at 600 nm), the ER changed from 4.0 to 8.0 (100% increase). The difference in ER values is due to the correlated decreases in both the QD and Alexa647 emission in the single excitation mode. Quenching of the QD by the cPC also reduces FRET to the Alexa647 because of the additional competing deactivation pathways of the QD (Figure 1B). When excited directly, the Alexa647 standard was unaffected by the photoconversion of the PC, resulting in a considerably larger ER change. A slight photobleaching was evident upon prolonged irradiation.

The dual-color psQD were cycled through the open-closed states by alternating lengthy (180 s) exposures to UV or visible light and monitoring the QD and Alexa647 emissions (Figure 2). The first irradiation with UV led to a significant decrease in the Alexa647 signal while subsequent cycles produced a more moderate decrease indicative of photobleaching (Figure 2A).

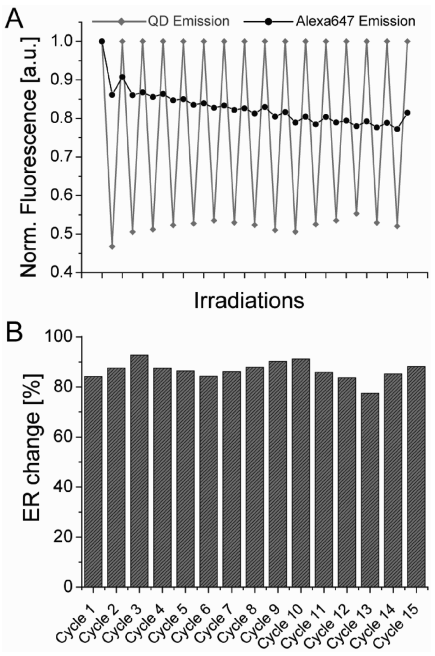

Figure 2. Spectroscopic monitoring of dual-color psQD cycled through open-closed states. Irradiation was for a continuous 180 s; 340 ± 10 nm (irradiance 1.1 mW cm^{-2}) and 545 ± 10 nm (irradiance 6.2 mW cm^{-2}). Temperature, 20 °C. (A) Emission of QD after each irradiation with excitation at 400 nm and detection at 550 nm. Emission of Alexa647 after each irradiation with excitation at 600 nm and detection at 666 nm. (B) Change in the ER during each cycle upon transition from the open to the closed state.

The latter effect could be minimized by eliminating oxygen from the solution with scavengers.[40] We attribute the initial step to redistribution of the Alexa647 from the more viscous interior to the exterior of the polymer coat, lowering the quantum yield due to facilitation of bond rotation.[40] The hypothesis was supported by an observed decrease in FRET from the QD to the Alexa647 (data not shown). The slight reversible steps in Alexa647 emission were independent of the state of the PC since they were observed when irradiating repeatedly at any given wavelength.

The QD did not exhibit photobleaching but some photobrightening was evident (compensated in Figure 2A by normalization). Photobrightening is an inherent property of many QDs[41,42] and we observed the phenomenon in naked QDs as well as polymer-coated QDs not functionalized by dyes. The influence of this phenomenon can be minimized by prior irradiation.[43] The photomodulation of QD fluorescence was robust over the 15 measured cycles in which the ER changed by 87 ± 4% (Figure 2B). Neither fatigue due to the photodegradation of the PC nor spontaneous thermal reversal of cPC was evident at room temperature. Thus, the state of the dual-color psQD was controlled solely via the selected mode of irradiation.

The dual-color psQD constitutes an inherently complex photophysical system by virtue of incorporating a QD donor and two distinct families of acceptors, one of which (the PC) undergoes photoinduced chemical transformations. As in the case of the Gen-1 psQDs,[22] the intermediate as well as the photostationary states of the PC groups generated with pulses of irradiation are heterogeneous in terms of the open/closed form distribution. It was necessary to again invoke the existence of two distinct acceptor populations differing in PC number and FRET efficiency as the simplest means for accommodating the combined absorbance and fluorescence transition data (Figure 1A,B; Supporting Information).

The original photophysical model[22] has been improved in the ensuing treatment, both in details of the formalism and the nature and number of parameters fit to the data.[22] We define two classes (1,2) of cPC FRET acceptors, class 1 arbitrarily being more FRET efficient. This feature is reflected in two parameters, the total number of groups per QD, $n_{1,2}$, and the FRET parameter, $\gamma_{1,2} = (R_o/r_{DA})^6_{1,2}$ where R_o is the Förster distance and r_{DA} the donor−acceptor distance, one or both of which can vary between the two classes. The assumptions within the model are that the photochromic parameters are the same for both populations such that in absence of FRET the photostationary state for the two PC populations is ∼0.22 upon exposure to UV (340 nm) irradiation. Ultraviolet light leads to photocyclization of oPC as well as photoreversion of cPC to oPC induced by direct excitation and indirectly via pcFRET (QD→cPC), whereas visible light induces photoreversion of cPC only by direct excitation.

Two coupled differential equations describe the time course of the oPC→cPC transition in the two acceptor populations to the photostationary state upon exposure to UV light ($c_{1,2}[t]$ = cPC$[t]$/QD; $o_{1,2}[t]$ = oPC$[t]$/QD; $n_{1,2} = c_{1,2}[t] + o_{1,2}[t]$):

$$c_1'[t] = k_{oc}Q_{oc,uv}\rho(n_1 - c_1[t]) - k_{co}Q_{co,uv}c_1[t] - k_{QD}Q_{co,vis}E_1[t]$$

dx.doi.org/10.1021/nl301093s | Nano Lett. XXXX, XXX, XXX−XXX

$$c_2'[t] = k_{oc}Q_{oc,uv}\rho(n_2 - c_2[t]) - k_{co}Q_{co,uv}c_2[t] - k_{QD}Q_{co,vis}E_2[t] \quad (1)$$

$$E_1[t] = \frac{c_1[t]\gamma_1}{1 + c_1[t]\gamma_1 + c_2[t]\gamma_2};$$

$$E_2[t] = \frac{c_2[t]\gamma_2}{1 + c_1[t]\gamma_1 + c_2[t]\gamma_2}; \quad n_{tot} = n_1 + n_2$$

$$Q_{co,uv} = \rho\left(\frac{1 - \alpha_{PS}}{\alpha_{PS}}\right)\left(\frac{\varepsilon_{oPC,uv}}{\varepsilon_{cPC,uv}}\right)Q_{oc,uv}$$

$$\text{quenching}\,\%[t] = 100(E_1[t] + E_2[t])$$

in which the rate constants k_{oc}, k_{co}, and k_{QD}, for the forward and reverse photoreactions, and the QD-induced (via pcFRET) reverse reaction respectively, are products of the known irradiance and absorption cross sections. The corresponding quantum efficiency values $Q_{oc,uv}$ (for photoconversion of the antiparallel conformer), $Q_{co,uv}$, $Q_{co,vis}$, and γ_1, γ_2, n_1 and n_2 are fitted variables, two of which are dependent; ρ, the fraction of the photocyclization-competent antiparallel isomer of oPC, equals 0.40 according to NMR determinations. This value is maintained by dynamic equilibration with the unreactive parallel isomer during photoconversion. The FRET efficiencies E_1 and E_2 and thus the extent of QD quenching (eq 1) vary in time and are interdependent due to the different time courses of c_1 and c_2.

We simultaneously fit the photoconversion to cPC ($c_{1,2}$) and the QD quenching (quenching %) as a function of the incremental UV irradiation dose using eq 1 and the *FindMinimum* routine of *Mathematica* (Wolfram Research). The fits are shown graphically in Figure 3 and Supporting Information S5 and the corresponding parameters are given in Table 1. The dual population model represents the data very well. Compared to the Gen-1 psQD, the new psQD has far fewer photochromic groups in total with only ~3 in class 1, yet the FRET parameters $\gamma_{1,2}$ are 4-fold and 8-fold greater, respectively, and the corresponding $(r_{DA}/R_o)_{1,2}$ 30% lower, resulting in a higher quenching efficiency in the photostationary state (50% vs 40%). The larger value of γ_1 in the dual psQD probably reflects a reduction in r_{DA} of the class 1 PC, which due to the added linker were placed up to 8.5 Å closer to the QD surface than in the Gen-1 psQD. The R_o computed for the QD-cPC pair is 4.1 nm in both systems, such that if we ascribe the differences in γ_1 (see Table 1) to positional effects alone, class 1 acceptors would be located 8.3 Å closer to the donor in the Gen-2 system, which is in excellent agreement with the stereochemical calculation. The linker may also result in better packing and orientation of the class 2 PC within the polymer/surface ligand matrix, accounting for the parallel reduction in γ_2.

The large absorption cross-section of the QD accounts for 84 and 75% of the A_{340} in the open and photostationary PC states, respectively and leads to the condition $k_{QD} \gg k_{oc}$, k_{co} reflected in the much faster equilibration (Figure 3B, inset) as well as in the displacement of the photostationary state to a very low steady-state value of $\alpha_{1,PS}$. Interestingly, both $\alpha_{1,PS}$ and $\alpha_{2,PS}$ were similar for the two psQD generations. The derived quantum efficiency of photocyclization (Q_{oc}, 0.4−0.5) significantly exceeds that for photoreversion ($Q_{co,uv}$, 0.1−0.2), which is also less efficient for excitation with visible light (or via FRET) ($Q_{co,vis}$, 0.01−0.02) compared to UV light. This result may be due to the intervention of additional, more efficient photoreversion pathways accessible to higher excited states in the latter case.[44] The reverse cycloreversion reaction, induced by visible light (546 nm) and analyzed by corresponding adjustment of the physical constants and starting condition of eq 1, yielded a slightly larger estimate for $Q_{co,vis}$ of 0.04 (Figure S5 in Supporting Information).

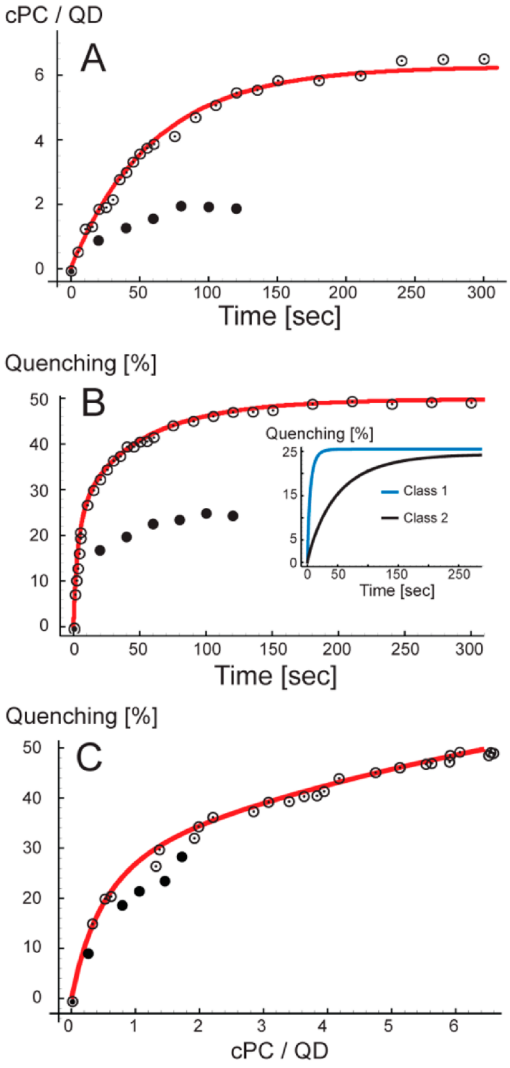

Figure 3. Photoconversion data and fits. Dual-color psQDs were irradiated with 340 ± 10 nm UV light, irradiance 1.1 mW cm^{-2} [⊙, Data]; [red line, Fit] or 365 nm UV light, irradiance 1.05 mW cm^{-2} [●, Data] for 1−15 s, absorbance and fluorescence spectra were recorded, and then a new pulse was applied. (A) Mean value of cPC molecules per QD as a function of irradiation time. (B) Fluorescence quenching of QD as a function of irradiation time. Inset: Quenching % corresponding to the two classes of acceptor as a function of time: blue line, Class 1; black line, Class 2. (C) Fluorescence quenching of QD as a function of mean value of cPC molecules per QD.

The above properties account for the nonintuitive phenomenon of very effective QD quenching despite the very low value of α_1. That is, the system exhibits a "ping-pong" or "autoreset" property in the presence of ≥1 class 1 or a larger number of class 2 cPC group(s). Excitation of the QD (favored under all conditions due to its very large absorption cross-section) is accompanied by a large probability of FRET transfer to the cPC. As a consequence, light emission of the QD is aborted and

dx.doi.org/10.1021/nl301093s | *Nano Lett.* XXXX, XXX, XXX−XXX

Table 1. Analysis of the UV-Induced Photoconversion and QD Quenching Kinetics[a]

psQD	Q_{oc}	$Q_{co,uv}$	$Q_{co,vis}$	n_1	n_2	γ_1	γ_2	k_{oc}	k_{co}	k_{QD}	$E_{1,PS}$	$E_{2,PS}$	$\alpha_{1,PS}$	$\alpha_{2,PS}$	$(r_{DA}/R_o)_1$	$(r_{DA}/R_o)_2$
Gen-2	0.44	0.14	0.015	3	32	6.6	0.08	0.01	0.08	2.2	0.26	0.24	0.02	0.20	0.7	1.5
	0.6	*3.0*	*1.4*	*1.2*	*1.6*	*4.8*	*2.0*									
Gen-1	0.52	0.17	0.015	14	81	1.5	0.01	0.01	0.08	0.8	0.32	0.03	0.03	0.18	0.9	2.1

[a]Gen-2, this study; Gen-1, PMA 6 PC 70 C12, from ref 22. Values in italics, relative deviations in % beyond which the increase in SSQ (sum of squares) of the fitting routine exceeds 10%. The units of k_{oc}, k_{co}, and k_{QD} are s^{-1}.

the acceptor PC reverts to the open state with fairly high efficiency.

Figure 3 also features data for UV photoconversion at 365 nm, a more accessible wavelength for fluorescence microscopy. Because of the less favorable oPC/cPC absorption cross-section ratio, the photostationary state was displaced to lower values of α_{PS}, and QD quenching diminished in accordance with the universal quantitative relation between quenching and cPC/QD content, established by exposure to 340 nm (Figure 3C).

We measured the fluorescence decay kinetics of the dual-color psQD in different states to confirm that the observed photomodulation was due to FRET. The decays of the parent QD and psQD were complex (Figure 4), requiring four

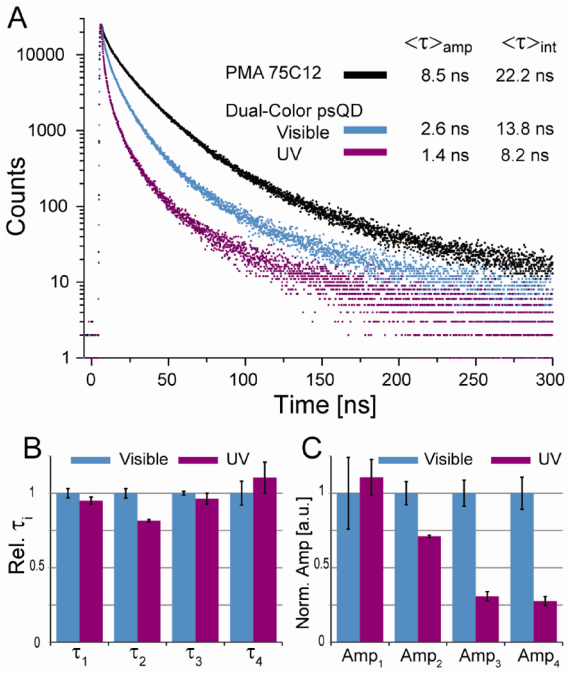

Figure 4. (A) Fluorescence-detected excited-state decays determined at 550 nm. (B) Individual decay constants normalized by the values for the oPC state. Absolute decay constants: oPC (initial state) τ_{1-4}, [0.48; 3.8; 12.7; 60 ns]; photostationary state τ_{1-4}, [0.45; 3.12; 12.2; 66 ns]. (C) Individual amplitudes, normalized by the oPC values. The amplitudes were converted to a common absolute scale by division by $\Sigma amp_{i,counts} \cdot \tau_i$ and multiplication by the steady-state spectrafluorimeter intensities. Relative amplitudes for the oPC state, amp_{1-4}, [1; 0.25; 0.10; 0.007] and for photostationary state; amp_{1-4}, [1; 0.17; 0.03; 0.002].

exponential components for the QD (and two for the Alexa647) to adequately represent the time course of excited state deactivation. In such Type II QDs, the exciton hole is confined to the core while the electron is delocalized in the core and first shell.[42] The outer liganded passivation shell accounts for a high quantum yield of core−shell−shell QDs.[35] The lower value of the final psQD indicates the presence of surface traps equilibrating with the radiative process of hole−electron recombination and/or the presence of defects and ligands contributing to nonradiative pathways.[45]

The psQD time-resolved decays of samples undergoing photoconversion cycles are best interpreted by examining the individual lifetimes and amplitudes (Figure 4), as well as two derived global means: amplitude weighed lifetime, $\langle\tau\rangle_{amp}$ and intensity weighed lifetime, $\langle\tau\rangle_{int}$ (Table 2). Analysis by an

Table 2. Amplitude Weighed Mean Lifetime $\langle\tau\rangle_{amp}$ and Intensity Weighed Mean Lifetime $\langle\tau\rangle_{int}$ of the Dual-Color psQD in the Two Photostationary States, and of Controls, Measured on a FluoroLog (Horiba Jobin Yvon) TCSPC System (Lifetime Values in ns)

QD detection[a]	polymer coated[c]	dual-color psQD oPC (Vis)	dual-color psQD oPC, cPC (UV)[d]
$\langle\tau\rangle_{amp}$	8.5 ± 0.1	2.6 ± 0.5	1.4 ± 0.1
$\langle\tau\rangle_{int}$	22.2 ± 0.2	13.8 ± 0.2	8.2 ± 0.2
Alexa647 detection[b]	in solution	dual-color psQD oPC (Vis)	dual-color psQD oPC, cPC (UV)[d]
$\langle\tau\rangle_{amp}$	1.28 ± 0.01	1.18 ± 0.01	1.14 ± 0.01
$\langle\tau\rangle_{int}$	1.17 ± 0.06	1.06 ± 0.05	1.02 ± 0.02

[a]Excitation with nanoLED N-320 nm and detection at 550 nm. [b]Excitation with nanoLED N-560 nm and detection at 660 nm. [c]CANdot CSS 540 nm QDs coated with amphiphilic polymer lacking PC and Alexa probe. [d]Photostationary state (oPC and cPC equilibrium) established by UV irradiation.

extended exponential $(\exp[-(t/\tau_{ext})^{\beta}])$[41,45] was also carried out but did not provide additional insights. FRET systems with donors presenting multiple decays are generally represented in terms of $\langle\tau\rangle_{amp}$ since for a given impulse response amplitude this quantity reflects the total emission under the decay curve.[46,47] In fact, $\langle\tau\rangle_{amp}$ diminished by 47 ± 3% (2.6 → 1.4 ns) in three successive oPC → cPC transitions, a value identical to that obtained from the steady-state emission and also indicative of a lack of undetected dark states.[46] The corresponding change in $\langle\tau\rangle_{int}$ was smaller (40%). The individual four decay constants (τ_{1-4}: ~0.5, 4, 13, 60 ns)[48] did not vary systematically during photocycling but the amplitudes, $amp_{2,3,4}$ strongly reflected the global quenching, decreasing by 30, 71, and 68%, respectively, upon photocyclization (Figure 4B,C). On the basis of the decay intensities, components 2 and 3 were the major contributors to the QD emission.

There was a significant decrease in the $\langle\tau\rangle_{amp}$ of QDs coated with an unmodified amphiphilic polymer upon passing to the dual-color psQD system. Previous investigations[49] have rationalized this effect in terms of FRET and/or screening processes but we propose that the coating efficiency plays a larger role in our system. A polymer only containing pendant alkyl chains will coat more efficiently than one carrying voluminous dyes such as PC and Alexa647. The Alexa647 probe exhibited a slightly shorter lifetime when conjugated to

dx.doi.org/10.1021/nl301093s | Nano Lett. XXXX, XXX, XXX−XXX

psQD than in solution but the sensitivity to PC photocyling was negligible.

In conclusion, we have prepared a water-soluble dual-color nanoparticle with ratiometric imaging capabilities. The technique is based on coating a QD with a dye-doped amphiphilic photochromic polymer providing solubility in aqueous media. The dual-color psQD are distinguished by small size (5.5 nm diameter with a 14 nm hydrodynamic diameter), biocompatibility, a broad excitation spectra, dual emission at 550 and 666 nm, a tunable emission ratio with up to 100% change upon photochromic switching, and distinct fluorescence lifetimes for the different components and states. A very advantageous feature of the psQD system is the prominent quenching of the QD exerted by low degrees of photoconversion. This effect, attributable to pcFRET as indicated above, should greatly facilitate achieving the modulation required for sensitive lock-in detection.[31]

The properties of the dual-color psQD should lead to manifold applications in cellular imaging, particular due to the greater sensitivity, selectivity, and background rejection afforded by the dual emission and photoswitchable ratiometric signals. We envision the potential of using laser light sources for precise control of the ER of single nanoparticles, as in single-particle tracking. Numerous combinations of dyes, sensors, and nanoparticles are feasible since the polymer preparation can be fine-tuned to obtain different functionalities as well as improving existing ones. For example, the addition of a linker to the PC group placed the FRET acceptor closer to the QD, such that the photochromic quenching of the psQD increased by 30% while the number of PC groups required decreased by 60% in comparison to the Gen-1 constructs. Because of their decay kinetics, the psQDs are also ideal for FLIM. Additional PC tailoring such as improved photoconversion and red-shifted spectra could further improve the utility of the nanoparticles in the cellular context, for example, in imaging strategies for pulse-chase experiments based on spatiotemporally structured illumination. The psQD probes may also be suited for applications in super-resolution microcopy.[5,50]

■ ASSOCIATED CONTENT

Supporting Information

Synthesis and characterization of PCahx; TEM images; details regarding the photophysical and computational data. This material is available free of charge via the Internet at http://pubs.acs.org.

■ AUTHOR INFORMATION

Corresponding Author

*E-mail: tjovin@gwdg.de.

Notes

The authors declare no competing financial interest.

■ ACKNOWLEDGMENTS

Elizabeth A. Jares-Erijman, the corresponding author and thesis supervisor of S.A.D., passed away during the final revisions of the manuscript. The surviving authors dedicate this publication to her memory and in acknowledgment of her inspiration, leadership, contributions, and outstanding personal qualities. We thank D. Arndt-Jovin and M. Konrad for valuable discussions, D. Riedel and G. Heim for the TEM images, NMR-Service, Georg-August-Universität (Göttingen, Germany) for NMR spectra, and the Department of Physical Biochemistry, MPIbpc, for the use of the TCSPC fluorimeter. This study was supported by the Max Planck Society (E J.-E., Partner Group grant; T.M.J and E.J.-E., Toxic Protein Conformation project), Argentine agencies ANPCyT, CONICET, UBA (E.J.-E.), and Cluster of Excellence 171 of the DFG Centre for the Molecular Physiology of the Brain (DFG CMPB). S.A.D was supported by the Deutscher Akademischer Austauschdienst (DAAD-Sandwich Doctorate Scholarship No. A/09/75106).

■ REFERENCES

(1) Fu, A.; Gu, W.; Larabell, C.; Alivisatos, A. P. *Curr. Opin. Neurobiol.* **2005**, *15*, 568−575.
(2) Delehanty, J. B.; Bradburne, C. E.; Susumu, K.; Boeneman, K.; Mei, B. C.; Farrell, D.; Blanco-Canosa, J. B.; Dawson, P. E.; Mattoussi, H.; Medintz, I. L. *J. Am. Chem. Soc.* **2011**, *133*, 10482−10489.
(3) Bruchez, M. P. *Curr. Opin. Chem. Biol.* **2011**, *15*, 775−780.
(4) Pinaud, F.; Clarke, S.; Sittner, A.; Dahan, M. *Nat. Methods* **2010**, *7*, 275−285.
(5) Leung, B. O.; Chou, K. C. *Appl. Spectrosc.* **2011**, *65*, 967−980.
(6) Yu, W. W. *Expert Opin. Biol. Ther.* **2008**, *8*, 1571−1581.
(7) Sperling, R. A.; Parak, W. J. *Philos. Trans. R. Soc. London, Ser. A* **2010**, *368*, 1333−1383.
(8) Zhang, F.; Ali, Z.; Amin, F.; Riedinger, A.; Parak, W. J. *Anal. Bioanal. Chem.* **2010**, *397*, 935−942.
(9) Erno, Z.; Yildiz, I.; Gorodetsky, B.; Raymo, F. M.; Branda, N. R. *Photochem. Photobiol. Sci.* **2010**, *9*, 249−253.
(10) Yildiz, I.; Tomasulo, M.; Raymo, F. M. *J. Mater. Chem.* **2008**, *18*, 5577−5584.
(11) Medintz, I. L.; Trammell, S. A.; Mattoussi, H.; Mauro, J. M. *J. Am. Chem. Soc.* **2004**, *126*, 30−31.
(12) Rogach, A. L.; Klar, T. A.; Lupton, J. M.; Meijerink, A.; Feldmann, J. *J. Mater. Chem.* **2009**, *19*, 1208−1221.
(13) Jares-Erijman, E. A.; Jovin, T. M. *Nat. Biotechnol.* **2003**, *21*, 1387−1395.
(14) Giordano, L.; Jovin, T. M.; Irie, M.; Jares-Erijman, E. A. *J. Am. Chem. Soc.* **2002**, *124*, 7481−7489.
(15) Jares-Erijman, E.; Giordano, L.; Spagnuolo, C.; Lidke, K.; Jovin, T. *Mol. Cryst. Liq. Cryst.* **2005**, *430*, 257−265.
(16) Giordano, L.; Vermeij, R. J.; Jares-Erijman, E. A. *Arkivoc* **2005**, 268−281.
(17) Irie, M. *Chem. Rev.* **2000**, *100*, 1685−1716.
(18) Irie, M. *Photochem. Photobiol. Sci.* **2010**, *9*, 1535−1542.
(19) Polyakova, S. M.; Belov, V. N.; Bossi, M. L.; Hell, S. W. *Eur. J. Org. Chem.* **2011**, *2011*, 3301−3312.
(20) Hirose, T.; Matsuda, K.; Irie, M. *J. Org. Chem.* **2006**, *71*, 7499−7508.
(21) Saitoh, M.; Fukaminato, T.; Irie, M. *J. Photochem. Photobiol., A* **2009**, *207*, 28−31.
(22) Díaz, S. A.; Menendez, G. O.; Etchehon, M. H.; Giordano, L.; Jovin, T. M.; Jares-Erijman, E. A. *ACS Nano* **2011**, *5*, 2795−2805.
(23) Pellegrino, T.; Manna, L.; Kudera, S.; Liedl, T.; Koktysh, D.; Rogach, A. L.; Keller, S.; Rädler, J.; Natile, G.; Parak, W. J. *Nano Lett.* **2004**, *4*, 703−707.
(24) Díaz, S. A.; Toscani, A. M.; Arndt-Jovin, D. J.; Jovin, T. M.; Jares-Erijman, E. A. Small Photostable Photoswitchable Quantum Dots as Nanotools for Live Cell Imaging. In *Nanotech*; NSTI, Ed.; CRC Press: Boston, USA, 2011; Vol. 3, pp 205−208.
(25) Zhang, F.; Lees, E.; Amin, F.; RiveraGil, P.; Yang, F.; Mulvaney, P.; Parak, W. J. *Small* **2011**, *7*, 3113−3127.
(26) Ruan, G.; Winter, J. O. *Nano Lett.* **2011**, *11*, 941−945.
(27) Zhu, L.; Wu, W.; Zhu, M.-Q.; Han, J. J.; Hurst, J. K.; Li, A. D. Q. *J. Am. Chem. Soc.* **2007**, *129*, 3524−3526.
(28) Chen, J.; Zhang, P.; Fang, G.; Yi, P.; Yu, X.; Li, X.; Zeng, F.; Wu, S. *J. Phys. Chem. B* **2011**, *115*, 3354−3362.
(29) Genovese, D.; Montalti, M.; Prodi, L.; Rampazzo, E.; Zaccheroni, N.; Tosic, O.; Altenhöner, K.; May, F.; Mattay, J. *Chem. Commun.* **2011**, *47*, 10975−10977.

(30) Osakada, Y.; Hanson, L.; Cui, B. *Chem. Commun.* **2012**, *48*, 3285−3287.
(31) Marriott, G.; Mao, S.; Sakata, T.; Ran, J.; Jackson, D. K.; Petchprayoon, C.; Gomez, T. J.; Warp, E.; Tulyathan, O.; Aaron, H. L.; Isacoff, E. Y.; Yan, Y. *Proc. Natl. Acad. Sci. U.S.A.* **2008**, *105*, 17789−17794.
(32) Colyer, R. A.; Lee, C.; Gratton, E. *Microsc. Res. Techniq.* **2008**, *71*, 201−213.
(33) Fernández-Argüelles, M. T.; Yakovlev, A.; Sperling, R. A.; Luccardini, C.; Gaillard, S.; Sanz Medel, A.; Mallet, J.-M.; Brochon, J.-C.; Feltz, A.; Oheim, M.; Parak, W. J. *Nano Lett.* **2007**, *7*, 2613−2617.
(34) Janczewski, D.; Tomczak, N.; Han, M.-Y.; Vancso, G. J. *Nat. Protoc.* **2011**, *6*, 1546−1553.
(35) Talapin, D. V.; Mekis, I.; Götzinger, S.; Kornowski, A.; Benson, O.; Weller, H. *J. Phys. Chem. B* **2004**, *108*, 18826−18831.
(36) Parak, W. J.; Pellegrino, T.; Plank, C. *Nanotechnology* **2005**, *16*, R9−R25.
(37) Clapp, A. R.; Medintz, I. L.; Mattoussi, H. *ChemPhysChem* **2006**, *7*, 47−57.
(38) Sadhu, S.; Patra, A. *ChemPhysChem* **2008**, *9*, 2052−2058.
(39) Algar, W. R.; Wegner, D.; Huston, A. L.; Blanco-Canosa, J. B.; Stewart, M. H.; Armstrong, A.; Dawson, P. E.; Hildebrandt, N.; Medintz, I. L. *J. Am. Chem. Soc.* **2012**, *134*, 1876−1891.
(40) Levitus, M.; Ranjit, S. *Q. Rev. Biophys.* **2010**, *44*, 123−151.
(41) Cooper, D. R.; Suffern, D.; Carlini, L.; Clarke, S. J.; Parbhoo, R.; Bradforth, S. E.; Nadeau, J. L. *Phys. Chem. Chem. Phys.* **2009**, *11*, 4298−4310.
(42) Carrillo-Carrion, C.; Cardenas, S.; Simonet, B. M.; Valcarcel, M. *Chem. Commun.* **2009**, 5214−5226.
(43) Llopis, M. V.; Rodríguez, J. C. C.; Martín, F. J. F.; Coto, A. M.; Fernández-Argüelles, M. T.; Costa-Fernández, J. M.; Sanz-Medel, A. *Nanotechnology* **2011**, *22*, 385703.
(44) Murakami, M.; Miyasaka, H.; Okada, T.; Kobatake, S.; Irie, M. *J. Am. Chem. Soc.* **2004**, *126*, 14764−14772.
(45) Schlegel, G.; Bohnenberger, J.; Potapova, I.; Mews, A. *Phys. Rev. Lett.* **2002**, *88*, 137401.
(46) Sillen, A.; Engelborghs, Y. *Photochem. Photobiol.* **1998**, *67*, 475−486.
(47) Wu, P. G.; Brand, L. *Anal. Biochem.* **1994**, *218*, 1−13.
(48) "Lifetimes" are inadequate terms for the reciprocal eigenvalues corresponding to excited state dynamics because they generally do not reflect the deactivation of distinct chemical species but rather of a network of excited states; the observed "amplitudes" are the eigenvectors.
(49) Niebling, T.; Zhang, F.; Ali, Z.; Parak, W. J.; Heimbrodt, W. *J. Appl. Phys.* **2009**, *106*, 104701.
(50) Dertinger, T.; Colyer, R.; Iyer, G.; Weiss, S.; Enderlein, J. *Proc. Natl. Acad. Sci. U.S.A.* **2009**, *106*, 22287−22292.

Modulation of a Photoswitchable Dual-Color Quantum Dot containing a Photochromic FRET Acceptor and an Internal Standard

Sebastián A. Díaz, Luciana Giordano, Thomas M. Jovin, Elizabeth A. Jares-Erijman

Supporting information

1. Synthesis and Characterization of PCahx

A. Synthesis of PCahx

6-amino-N-(3-(3,3,4,4,5,5-hexafluoro-2-(2-methylbenzo[b]thiophen-3-yl) cyclopent-1-enyl)-2-methylbenzo[b]thiophen-6-yl) hexanamide.

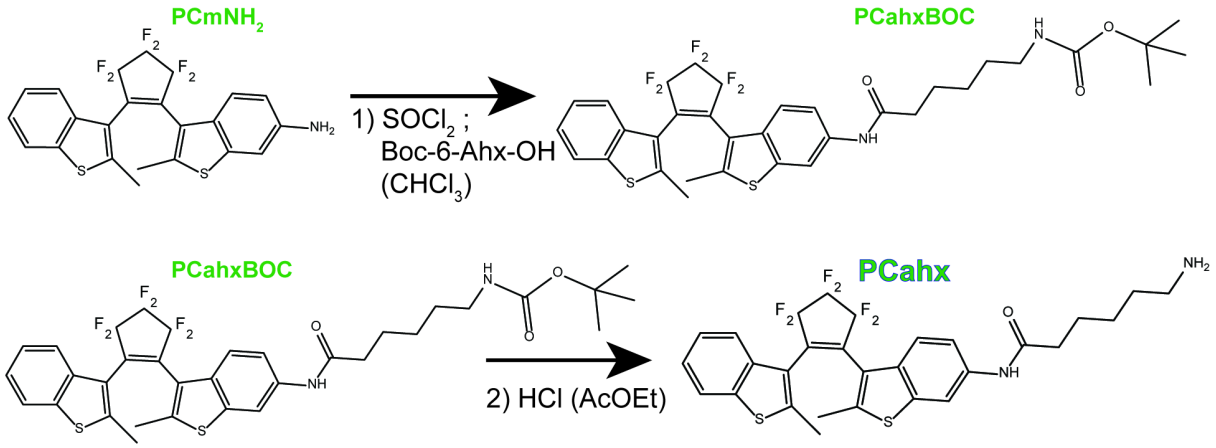

Figure S1. Synthetic scheme for PCahx

1) Commercially available 6-(tert-butoxycarbonylamino) hexanoic acid (46 mg, 200 µmoles, Sigma-Aldrich CAS: 6404-29-1), was added to a flask that had been previously dried and flushed with argon. Thionyl chloride (20 µl, 275 µmoles, CAS:7719-09-7) was added, the flask was flushed with argon and allowed to react for 30 min at 50 ºC. The flask was dried in a rotovap system to obtain freshly formed tert-butyl 6-chloro-6-oxohexylcarbamate (CAS: 903891-59-8).

A solution containing $PCmNH_2$ (50 mg, 100 µmoles) prepared in the lab[1] was dissolved in dry $CHCl_3$. The solution was added to the dry flask containing the tert-butyl 6-chloro-6-oxohexylcarbamate and allowed to react at 30 ºC for 2 h. The reaction was neutralized with NaOH solution and the crude was extracted with CH_2Cl_2, a greenish-brownish oil was obtained. Purification was performed on a silica gel column with cyclohexane:ethyl acetate

(90:10) mobile phase. The intermediate product tert-butyl 6-(3-(3,3,4,4,5,5-hexafluoro-2-(2-methylbenzo[b]thiophen-3-yl)cyclopent-1-enyl)-2-methylbenzo[b]thiophen-6-ylamino)-6-oxohexylcarbamate was obtained (38 mg, 54.4 μmoles) as a pink oil.

^{1}H NMR (500 MHz, $CDCl_3$) δ 1.25 (dd, *2*.04H, CH2-CH2-CH2), 1.41 (s, 11H, C-(CH3)3), 1.68 (m, *2*.81H, CH2), 1.75 (dd, *2*.18H, CH2), 2.13 (*s,* 2.80H, CH3 ap), 2.16 (s, 2.89H, CH3 ap), 2.35 (t, *2*.02H, NH-CO-CH2), 2.43 (2*s,* 3.3H, CH3 p), 3.10 (bp, *2*.36H, CH2-NH-CO), 6.85-7.70 (m, 6H, ArH), 8.18 (*s,* 0.35H, H-7 p), 8.22 (*s,* 0.65H, H-7 ap).
Parallel (p) to antiparallel (ap) isomers 40:60

2) The BOC protective group was released from the aliphatic amine by addition of 20% fuming HCl in ethyl acetate for 10 min at room temperature. The reaction was quenched with NaOH and extracted with CH_2Cl_2. The product was purified by creating a silica gel filter, impurities were removed with washes of cyclohexane: ethyl acetate (from 100% cyclohexane to 100% ethyl acetate) and then the product was obtained by eluting with DMF. Solvent was evaporated in a rotovap system and the final product, 6-amino-N-(3-(3,3,4,4,5,5-hexafluoro-2-(2-methylbenzo[b]thiophen-3-yl) cyclopent-1-enyl)-2-methylbenzo[b]thiophen-6-yl) hexanamide (20 mg, 33μmoles) was obtained as a pink/orange oil.

^{1}H NMR (400 MHz, $CDCl_3$) δ 1.25 (m, *1*.94H, CH2-CH2-CH2), 1.51 (m, *2*.30H, CH2), 1.72 (m, *2*.07H, CH2), 2.13 (*s,* 1.20H, CH3 ap), 2.16 (s, 1.18H, CH3 ap), 2.34 (t, *2*.04H, NH-CO-CH2), 2.43 (2*s,* 2.66H, CH3 p), 2.71 (m, *2*.00H, CH2-NH2), 6.85-7.70 (m, 6H, ArH), 8.18 (*s,* 0.35H, H-7 p), 8.22 (*s,* 0.65H, H-7 ap).
Parallel (p) to antiparallel (ap) conformers 40:60

B. Characterization of PCahx

The analysis is based on the quantative formalism for the photostationary stage presented in our previous publications.[1, 2] Structural similarities to a previously studied diheteroarylethene, [4-((3-(3,3,4,4,5,5-hexafluoro-2-(2-methylbenzo[*b*]thiophene-3-yl)cyclopent-1-en-1-yl]-2-methylbenzo[*b*]thiophene-6-yl)amino)-4-oxobutanoic acid],[1] suggested that the photophysical properties would be comparable. The values calculated for the PCahx are consistently within the expected range as detailed below. A sample of PCahx was dissolved in $CDCl_3$ and ^{1}H NMR (400 MHz) was carried out on the sample in its open and photostationary forms.

Table S1. Integrated values for ^{1}H NMR signals of interest in PCahx

State	Peaks (chemical shift, ppm)		
	1.99	2.15	2.43
open	3922	4459	3724
photostationary	4964	3401	2955

The spectral changes display the same chemical shifts as in our previous publication. The methyl peaks presented the clearest area for quantification, preferable to the complex aromatic region. Irradiation at 340 nm led to decreases of 24% and 21%, of the CH_3 ap (2.13 and 2.16 ppm) and CH_3 p (2.43 ppm) hydrogens respectively, as well as an increase of the 1.99 ppm peak. The increase in the 1.99 peak is hard to quantify due to a partial overlap with another pre-existing peak. We conclude that in the photostationary state, α_{PS} = 0.22 of the photochromic acceptor is in the closed form. We assumed that the same functional photoconversion applied to the PC- in the polymer within the dual-color psQDs, i.e. in the hypothetical absence of intervention by the QD.

Solutions of known concentrations of PCahx were prepared in $CHCl_3$ and EtOH. Assuming the validity of Lambert-Beer conditions, the extinction coefficients were calculated by applying the established 22% photoconversion in the photostationary state. The spectra are presented in Figure S2 and the results in Table S2.

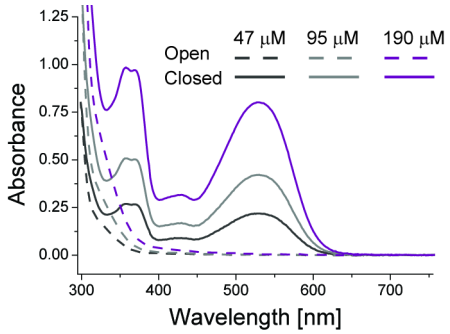

Figure S2. Absorbance spectra of PCahx solutions of varying concentrations in chloroform. The open form (- -) shown as dashed lines and the closed (photostationary) state (—) as solid lines. Not all the concentrations used to calculate the extinction coefficients are presented in the figure.

Table S2. Extinction coefficients (M^{-1} cm^{-1}) at different wavelengths of interest in the open and closed states of PCahx

State	Wavelength [nm]				
	340	365	400	540	550
Open (oPC)	2000	665	175	25	20
Closed (cPC)	9100	19000	5730	17530	16500

An isosbestic point occurs at 301 nm in EtOH. Using equation S1 and the values in Table S3 we calculated α_{PS} for the photostationary state in EtOH. The value was 0.22, corroborating the determination by NMR spectroscopy.

$$\alpha_{PS} = -\left(\frac{\varepsilon_{-}^{540}}{\varepsilon_{+}^{540} - \varepsilon_{-}^{540}}\right) + \left(\frac{\varepsilon^{isos}}{\varepsilon_{+}^{540} - \varepsilon_{-}^{540}}\right)\left(\frac{A_{PS}^{5}}{A^{isos}}\right) \quad [S1]$$

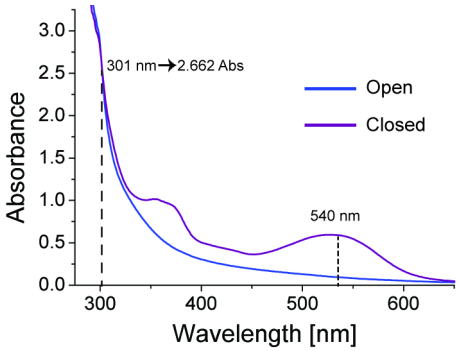

Figure S3. Absorbance of PCahx solution in ethanol in the open and open/closed (photostationary) states.

Table S3. Extinction coefficients and absorbance values of PCahx in EtOH.

Solvent	ε_{-}^{540} ($M^{-1}cm^{-1}$)	ε_{+}^{540} ($M^{-1}cm^{-1}$)	ε^{isos} ($M^{-1}cm^{-1}$)	A_{PS}^{535}	A^{isos}	α_{PS}
EtOH	25[a]	17530[a]	17250	0.592	2.662	0.22

a. Values previously calculated using $CHCl_3$ as solvent.

2. TEM Images

Samples were of ~0.1 µM concentration. They were placed on a carbon grid and imaged with a Philips 120 kV BioTwin microscope equipped with a 1024×1024 pixel GATAN CCD camera (Gatan, Inc.).

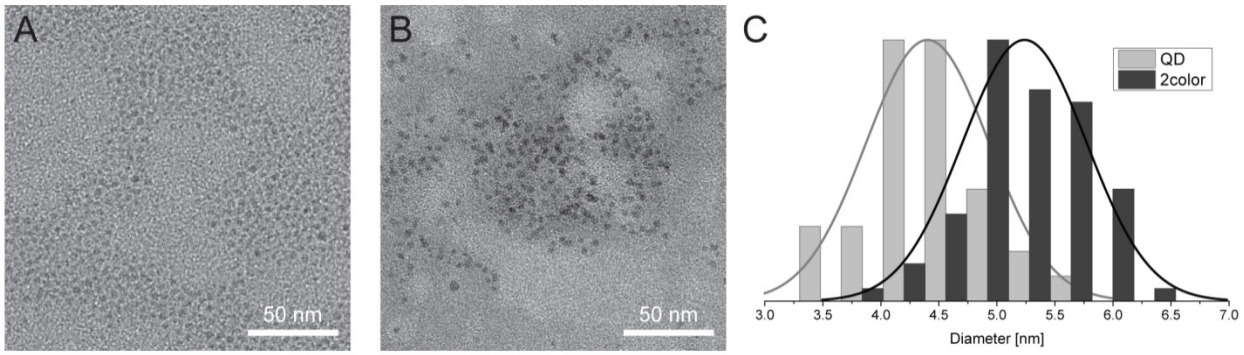

Figure S4. TEM images (A) CANdot® Series A CSS 540 nm, CAN GmbH, Hamburg in hexane as provided by manufacturer. (B) Dual-color psQDs in SBB 50 mM. (C) Size distributions of samples (N > 70QDs)

The addition of the polymer coating to the QDs leads to an increase in the mean diameter from 4.4 ± 0.5 nm to 5.3 ± 0.5 nm. Outliers, >2σ, were assigned to aggregates and eliminated from calculations.

3. Photophysical Data and Evaluations

In the experimental set-up for the determination of the kinetic constants of photoconversion, photoswitching of the PC probe was achieved by irradiation of the dual-color psQD with UV light (340 ± 10 nm, 1.1 mW cm^{-2}) and, in the case of the photoreversal reaction(Figure S5), by visible/green light (545 ± 10 nm, 6.2 mW cm^{-2}). Measurements were realized in 100 µl microcuvettes with a 10 mm optical path on a Cary 100 UV-Vis Spectrophotometer and a Cary Eclipse Fluorimeter (Varian). Samples were allowed to reach room temperature and were irradiated for a short time (normally 30 s) with green light to assure that the PC moeties were in the open state. Short pulses (~ 1-15 sec) of UV irradiation were utilized, with spectral determinations after each irradiation, until the photostationary stage was achieved.

The PC conversion and QD quenching data (Figure 3, UV irradiation; Figure S5, visible light irradiation) were fitted by creating a composite difference function based on evaluation of the differential equations for the closed forms of class 1 and 2 PC (Equation 1) and applying the FindMinimum subroutine of *Mathematica* (Wolfram Research) with a minimal least squares criterium for convergence. The fitted parameters are those given in the first row of Table 1 with $Q_{oc,uv}$ linked to $Q_{co,uv}$ as indicated in the text. The FindMinimum subroutine does not provide error estimations. A rough estimation of parameter sensitivity was based on systematic relative perturbation of each fitted quantity, as indicated in Table 1.

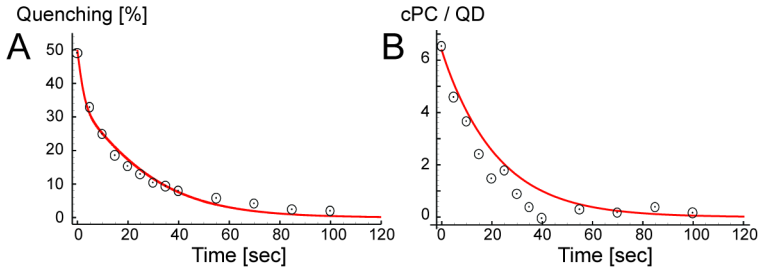

Figure S5. Photoreversal of psQD by irradiation with visible light. Dual-color psQDs in the photostationary state were irradiated with successive 5-10 s pulses of visible light (5-10 s, 545 ± 10 nm, irradiance 6.2 mW cm^{-2}). Absorbance and fluorescence spectra were recorded after each pulse. (A) Fluorescence quenching of QD as a function of irradiation time. [⊙, Data]; [—, Fit] (B) Mean value of cPC molecules per QD as a function of irradiation time. [⊙, Data]; [—, Fit].

References

1. Díaz, S. A.; Menendez, G. O.; Etchehon, M. H.; Giordano, L.; Jovin, T. M.; Jares-Erijman, E. A. *ACS Nano* **2011,** 5, 2795-2805.

2. Giordano, L.; Jovin, T. M.; Irie, M.; Jares-Erijman, E. A. *J. Am. Chem. Soc.* **2002,** 124, 7481-9.